3576–3587 Nucleic Acids Research, 2013, Vol. 41, No. 6 Published online 7 February 2013
doi:10.1093/nar/gkt056

Single-molecule sorting reveals how ubiquitylation affects substrate recognition and activities of FBH1 helicase

Tokiha Masuda-Ozawa[1,2], Trish Hoang[1], Yeon-Soo Seo[3], Lin-Feng Chen[1] and Maria Spies[1,2,4,5,*]

[1]Department of Biochemistry, University of Illinois at Urbana-Champaign, Urbana, IL 61801, USA, [2]Howard Hughes Medical Institute, University of Illinois at Urbana-Champaign, Urbana, IL 61801, USA, [3]Department of Biological Sciences, National Creative Research Initiative Center for Cell Cycle Control, Korea Advanced Institute of Science and Technology, Daejeon 305-701, South Korea, [4]Center for Biophysics and Computational Biology, University of Illinois at Urbana-Champaign, Urbana, IL 61801, USA and [5]Department of Biochemistry, University of Iowa, Iowa City, IA 52242, USA

Received November 26, 2012; Revised January 8, 2013; Accepted January 10, 2013

ABSTRACT

DNA repair helicases function in the cell to separate DNA duplexes or remodel nucleoprotein complexes. These functions are influenced by sensing and signaling; the cellular pool of a DNA helicase may contain subpopulations of enzymes carrying different post-translational modifications and performing distinct biochemical functions. Here, we report a novel experimental strategy, single-molecule sorting, which overcomes difficulties associated with comprehensive analysis of heterologously modified pool of proteins. This methodology was applied to visualize human DNA helicase F-box–containing DNA helicase (FBH1) acting on the DNA structures resembling a stalled or collapsed replication fork and its interactions with RAD51 nucleoprotein filament. Individual helicase molecules isolated from human cells with their native post-translational modifications were analyzed using total internal reflection fluorescence microscopy. Separation of the activity trajectories originated from ubiquitylated and non-ubiquitylated FBH1 molecules revealed that ubiquitylation affects FBH1 interaction with the RAD51 nucleoprotein filament, but not its translocase and helicase activities.

INTRODUCTION

Functional diversity and the dynamic nature of the eukaryotic proteome are highly enhanced by post-translational modifications (PTMs) (1). Activity switching in DNA repair enzymes is often controlled by reversible PTMs, including phosphorylation, ubiquitylation, sumoylation and poly (ADP-ribozyl)ation (2). These chemical modifications regulate activities, localizations and interactions of the proteins, their integration into larger macromolecular assemblies and, ultimately, the selection of a cellular pathway. It is foreseeable that in some cases, a few or even a single-protein molecule carrying a particular array of modifications could decide a cell fate.

A number of techniques are available for producing mimetics of post-translationally modified proteins for biochemical and structural studies (3). The alternative is to separate an endogenously modified protein from the unmodified counterparts. These approaches have been successfully implemented in deciphering the roles of PTMs in the DNA repair proteins [see for example (4,5)], but they are laborious and non-optimal when the protein availability is limiting, when multiple PTMs are stochastically combined within the same protein or when only a small fraction of the protein is modified.

To expedite the quantification, analysis and comparison of distinct post-translationally modified pools of a protein, we developed a technique to simultaneously, but separately, evaluate activities of the modified and unmodified proteins extracted from the human cells. Human F-box–containing DNA helicase (FBH1) was used as a model to establish and evaluate this methodology.

FBH1 helicase both promotes homologous recombination during re-establishment of blocked replication forks (6) and acts as an anti-recombinase by controlling formation of toxic recombination intermediates (7–10). In its anti-recombinase mode, FBH1 is one of the mammalian candidates for the role of yeast Srs2 helicase (9), an anti-recombinogenic helicase that promotes Rad51 nucleoprotein filament disassembly by accelerating

*To whom correspondence should be addressed. Tel: +1 319 335 3221; Fax: +1 319 335 9570; Email: maria-spies@uiowa.edu

Rad51-mediated adenosine triphosphate (ATP) hydrolysis (11). Although having a moderate effect on chromosomal break repair in vertebrate cells (6,12), FBH1 is important for cellular recovery from decatenation stress and for restoration of mitotic progression (13).

Pro- and anti-recombinogenic functions may require FBH1 to rapidly switch between different activities. Similar to other helicases and helicase-like nucleic acid translocation motors [reviewed in (14–17)], FBH1 converts the energy of ATP into directional movement along DNA and separation of the DNA duplex (18,19).

In addition to SF1 helicase motor, FBH1 includes a large N-terminal extension containing an F-box motif, which serves as an adaptor for the Skp1, Cul1 and Roc1 components of E3 ubiquitin ligase (18,20) (Figure 1A). Chiolo *et al.* (9) proposed that FBH1 undergoes a DNA damage-induced self-degradation, which controls FBH1 abundance. Self-ubiquitylation of FBH1 may also play a regulatory role by modifying the helicase and/or translocase activities of FBH1 or by affecting its protein–protein interactions.

Here, we developed and applied a single-molecule sorting technique to quantify, as well as simultaneously probe and distinguish, activities of ubiquitylated and non-ubiquitylated FBH1 molecules. The basis of this approach is to surface-tether the helicase molecules expressed and biotinylated in the human cells. We then use total internal reflection fluorescence microscopy (TIRFM) (21) to follow the activities of each individual surface-tethered molecule over multiple cycles of binding and rearrangement of fluorescently labeled DNA substrates or nucleoprotein complexes. The presence of poly-ubiquitin chains on some FBH1 molecules is then revealed by fluorescence staining and is correlated to substrate binding, translocation and unwinding activities even when only a small fraction of helicase molecules are modified.

Using this technique, we probed the two activities most critical for FBH1 cellular functions: helicase activity, and its interaction with RAD51 nucleoprotein filament, a potential target of the FBH1 anti-recombinogenic function. We first analyzed the helicase activity of FBH1 on a set of DNA substrates representing different features of a stalled or a collapsed replication fork, where FBH1 helicase displays *bona fide* 3′–5′ helicase activity, i.e. the physical separation of the duplex into its component single strands, as well as a repetitive shuttling behavior similar to that observed for other SF1 helicases (22,23). Because RAD51 participates in repair and restart of both stalled and collapsed replication forks (24), we probed the interaction between FBH1 and RAD51 nucleoprotein filament. Notably, poly-ubiquitylation virtually abolished RAD51 nucleoprotein filament binding by FBH1, but it had no significant effect on duplex separation or translocation activity of FBH1.

MATERIALS AND METHODS

Constructs for expression, biotinylation and ubiquitylation of FBH1 helicase

Human *FBH1* gene was amplified from pcDNA3–FLAG–FBH1 (18) using primers to incorporate the FLAG epitope (DYKDDDDK) on the N-terminus and BAP sequence on the C-terminus. Then, *FLAG–FBH1–BAP* was re-cloned into the KpnI and EcoRV sites of pcDNA3 vector (Invitrogen). The BirA gene from *Escherichia coli* K-12 strain was cloned into BamHI and NotI sites of pcDNA3. The ubiquitylated (Ub) pcDNA3–HA vector for expression of HA-tagged ubiquitin is described in the study conducted by Lamb *et al.* (25).

FBH1 expression and purification

HEK293T cells were grown in the Dulbecco's Modified Eagle's Medium (Invitrogen) supplemented with 10% fetal bovine serum, 1 mM sodium pyruvate, 1% penicillin and 1% streptomycin at 37°C in the presence of 5% CO_2. Cells were transiently transfected for 24 h using polyethylenimine method (26,27). One microgram per microliter of branched polyethylenimine (MW: 25 000; Sigma-Aldrich) was used with 1 μg/μl of plasmid. To biotinylate FBH1 helicase, HEK293T cells were co-transfected with pcDNA3–FLAG–FBH1–BAP and pcDNA3–BirA at 1:1 ratio. Biotin (Sigma-Aldrich) was added into medium to 100 μM of final concentration. For co-expression of biotinylated FBH1 (FBH1–bio) and HA-tagged ubiquitin, cells were transfected with pcDNA3–FLAG–FBH1–BAP, pcDNA3–BirA and pcDNA3–HA–Ub at 1:1:1 ratio. Cells were harvested with Trypsin–EDTA (ethylenediaminetetraacetic acid) (Fisher scientific). Cells were washed with phosphate-buffered saline (VWR international), resuspended in the ice-cold lysis buffer [50 mM HEPES (pH 7.4), 250 mM NaCl, 1 mM EDTA, 0.1% Tween20 (Sigma-Aldrich), 10% glycerol and 1 mM phenylmethanesulfonyl fluoride] and incubated at 4°C for 30 min. After centrifugation, clarified cell lysate was mixed with anti-FLAG agarose beads (Sigma-Aldrich) equilibrated with lysis buffer and then incubated at 4°C for 2 h. Beads were then washed with lysis buffer, resuspended in the elution buffer [lysis buffer with 150 μg/ml of 3× FLAG peptides (Sigma-Aldrich)] and incubated at 4°C for 30 min. Eluted protein was immediately divided into small aliquots and preserved at −80°C.

Cloning of the F-box–containing N-terminal domain

The sequence encoding F-box–containing N-terminal domain ($FBH1^{NTD}$) was amplified using a pair of forward (5′-TTTTTTTTTTCATATGGCCAAAAGCAATTCTGTTG-3′) and reverse (5′-TTTTTTTTTTCTCGAGTTACTTATCGTCGTCATCCTTGTAGTCTTTTGTGGCCTGAGTG-3′) primers. Underlined sequences are the recognition sites for NdeI and XhoI restriction enzymes, respectively. The NdeI–$FBH1^{NTD}$–XhoI fragment was ligated into pET-15 b (Merck KGaA, Germany) and transformed into *E. coli* [Rosetta pLysS (Merck) containing pChaperone plasmid (gift from A. Mazin, Drexel University College of Medicine, PA, USA)].

Expression and Purification of Recombinant $FBH1^{NTD}$

$FBH1^{NTD}$ overexpression in *E. coli* was induced with 0.05 mM isopropyl β-D-1-thiogalactopyranoside at 16°C

for 24 h. Cell pellets were resuspended in lysis buffer [50 mM potassium phosphate (pH 7.4), 400 mM KCl, 1% Triton X100, 50 mM imidazole, 50 mM sucrose, 5 mM β-mercaptoethanol (β-Me) and 10% glycerol with protease inhibitors]. Cells were lysed by sonication, and then the lysate was clarified by centrifugation and filtration. A 5-ml HiTrap Chelating HP column (GE Healthcare UK Ltd, UK) charged with $NiSO_4$ was equilibrated in buffer Ni-1 [50 mM potassium phosphate (pH 7.4), 500 mM KCl, 50 mM imidazole, 5 mM β-Me, 50 mM sucrose and 10% glycerol]. The clarified lysate was applied to the column. The column was then washed extensively with buffer Ni-1, buffer Ni-2 [50 mM potassium phosphate (pH 7.4), 50 mM KCl, 50 mM imidazole, 5 mM β-Me and 10% glycerol], Ni-3 [50 mM potassium phosphate (pH 7.4), 50 mM KCl, 60 mM imidazole, 5 mM β-Me and 10% glycerol] and buffer Ni-3 containing 4 mM ATP and 10 mM $MgCl_2$. Proteins were eluted over linear gradient of 60–300 mM of imidazole. The peak fractions were pooled and applied to 5-ml HiTrap heparin column equilibrated in buffer A(H) [50 mM Tris–HCl (pH 7.5), 50 mM NaCl, 1 mM EDTA, 1 mM dithiothreitol (DTT) and 10% glycerol]. The proteins were eluted over linear gradient of 0–100% of buffer B(H) [50 mM Tris–HCl (pH 7.5), 1 M NaCl, 1 mM EDTA, 1 mM DTT and 10% glycerol]. The fractions containing $FBH1^{NTD}$ were pooled and dialyzed overnight against buffer A(Q) [50 mM Tris–HCl (pH 8.0), 50 mM NaCl, 1 mM EDTA, 1 mM DTT and 10% glycerol]. The dialyzate was loaded into Mono-Q (GE healthcare) column equilibrated in buffer A (Q). The proteins were eluted over a linear gradient of 0–25% of buffer B (Q) [50 mM Tris–HCl (pH 8.0), 2 M NaCl, 1 mM EDTA, 1 mM DTT and 10% glycerol]. Fractions containing $FBH1^{NTD}$ (Figure 4A) were aliquoted and stored at −80°C. Concentration of the protein was determined spectrophotometrically using $\varepsilon_{280} = 58745\,M^{-1}\,cm^{-1}$ calculated with EXPASY tools (http://ca.expasy.org/tools/).

DNA substrates

Oligonucleotides, which were used to anneal the DNA substrates, were purchased from IDT. Mixture of oligonucleotides at 3 μM (molecules) in a buffer containing 10 mM Tris–HCl (pH 7.0) and 100 mM NaCl was denatured at 95°C for 5 min and allowed to cool down slowly for 2 h in the heating block. Fluorescently-labeled DNA substrates were preserved at 4°C. The sequence of all oligonucleotides and modifications is shown in the Supplementary Tables S1 and S2.

ATPase assay

ATP hydrolysis was monitored using spectroscopic assays in which ATP hydrolysis and regeneration was coupled to nicotinamide adenine dinucleotide (NADH) oxidation through activities of pyruvate kinase (PK) and lactic dehydrogenase (LDH) (28). The absorbance of NADH at 340 nm was monitored at 25°C using Cary 300 BioUV Spectrophotometer (Agilent technologies, CA, USA) in a kinetics mode. The reaction mixture consisted of 20 mM Tris–HCl (pH 7.5), 3 mM $MgCl_2$, 1 mM DTT, 0.2 mg/ml of NADH, 2 mM phosphoenol pyruvate, 1× LDH/PK (28.8 U/ml of LDH and 37.24 U/ml of PK) and 1 mM ATP. One hundred and thirty-seven microliters of reaction buffer were pre-incubated in the cuvettes for 1 min followed by addition of 10 μl of elution fraction containing FBH1–bio. After 4 min of incubation, the reaction was initiated by addition of 1 μM (nucleotides) of poly $(dT)_{100}$.

Bulk helicase assay

Helicase activity of FBH1 was examined by monitoring fluorescence change of Cy3 and Cy5 dyes incorporated into partial duplex (PD) (10 nM). The DNA unwinding was monitored at 25°C using Cary Eclipse Fluorescence Spectrophotometer (Varian/Agilent). Cy3 dye was excited at 530 nm, and emissions were recorded at 560 nm for Cy3 and at 663 nm for Cy5, simultaneously. The reaction mixtures containing 50 mM Tris–HCl (pH 7.5), 150 mM NaCl and 3 mM $MgCl_2$ were pre-incubated for 1 min followed by addition of 10 μl of elution fraction containing FBH1. After 1-min incubation, unwinding was initiated by adding 1 mM ATP.

Analysis of DNA–$FBH1^{NTD}$ interactions

DNA binding to $FBH1^{NTD}$ was monitored by following the intrinsic protein fluorescence. Measurements were carried out using Cary Eclipse fluorescence spectrophotometer (Varian/Agilent). The tyrosine and tryptophan residues were excited at 280 nm, and their emissions were monitored at 320 nm. The reaction buffer was 30 mM Tris–HCl (pH 8.0) and 1 mM DTT. The emission spectrum of free protein (100 nM $FBH1^{NTD}$) was examined and followed by 1.5 μM (in nucleotides) titration of DNA substrates, ssDNA [$(dT)_{100}$] and linear dsDNA. The fluorescence quenching Q (%) was calculated as:

$$Q(\%) = \frac{100 \times (F_0 - F)}{F_0}$$

where F_0 is the fluorescence of free protein, and F is the fluorescence in the presence of DNA.

Analysis of $FBH1^{NTD}$–RAD51 interactions

RAD51 protein was expressed using pET11–RAD51 plasmid (29) (gift from A. Mazin, Drexel University College of Medicine, PA, USA) in the AB1157-Δ*rec*A-(DE3) strain containing Rosetta and pChaperone plasmids and was purified as described in the study conducted by Tombline and Fishel (30). The pull-down experiments were carried out as described by Spies and Kowalczykowski (31). Briefly, 2 μM of 6× his-tagged $FBH1^{NTD}$ was pre-incubated with RAD51 at indicated concentrations in 40 μl reaction for 20 min at room temperature in the binding buffer (20 mM Tris, pH 8.0, 5 mM β-mercaptoethanol, 0.5% Triton X-100, 30 mM imidazole, 5 mM $MgCl_2$ and 5 mM $CaCl_2$). The reaction was added to the washed Ni-Magnetic Agarose beads (Qiagen) and incubated for 45 min at room temperature with gentle

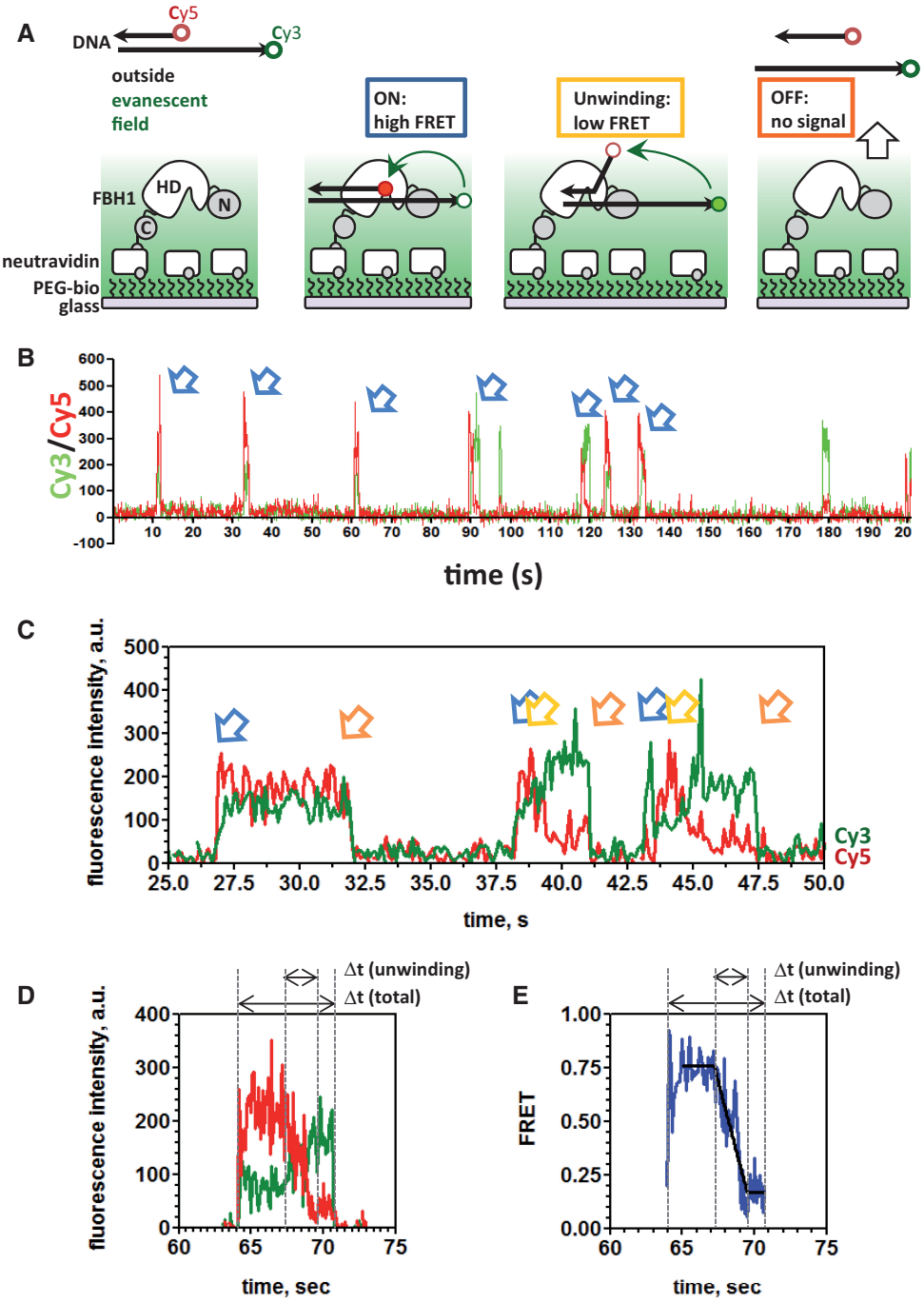

Figure 1. Surface-tethered FBH1 helicase displays a *bona fide* unwinding activity. (**A**) Schematic representation of TIRFM-based assay for analysis of DNA binding and unwinding by the individual surface-tethered helicases molecules. FBH1 is immobilized on the surface of the microscope flow cell illuminated with a 530-nm evanescent wave generated by TIR. DNA substrate molecules contain two fluorescence dyes (Cy3, donor; Cy5, acceptor). Both dyes are invisible unless found within the evanescent field because of association with the surface-tethered helicase (ON state). In the presence of ATP, FBH1-mediated unwinding of the duplex region of the DNA substrate results in gradual decrease in the FRET efficiency. Substrate dissociation results in a loss of the signal. (**B**) Activity of an individual surface-tethered FBH1 molecule was monitored >200 s in the presence of 1 mM ATP and PD1. Each spike in the fluorescence intensities of Cy3 (green) and Cy5 (red) marked by the blue arrow corresponds to binding and rearrangement of a new DNA substrate. Only events featuring fluorescence of both Cy3 and Cy5 dyes were analyzed. Each experiment yielded 200–600 trajectories originated from individual surface-tethered FBH1 molecules similar to the one depicted here. (**C**) A magnified fragment of a representative fluorescence trajectory depicting three consecutive events where FBH1 binds and unwinds PD1. Blue, orange and yellow arrows represent binding, dissociation and unwinding, respectively. (**D**) An individual unwinding event. (**E**) The Cy3 and Cy5 signals from the event depicted in the panel D and converted into a FRET trajectory, which can be divided into three sections: initial binding of the DNA substrate to FBH1 (flat portion), active unwinding of the duplex (linear decrease in FRET efficiency), dissociation of the displaced Cy5-labeled oligo, whereas the Cy3 (translocating) oligo remains bound to the FBH1.

mixing. The unbound proteins were removed by washing beads three times with 50 µl of binding buffer. The bound proteins were eluted with 20 µl of elution buffer (20 mM Tris, pH 8.0, 5 mM β-mercaptoethanol, 0.5% Triton X-100, 300 mM imidazole, 5 mM $MgCl_2$ and 5 mM $CaCl_2$). The proteins were resolved in 15% sodium dodecyl sulfate–polyacrylamide gel electrophoresis (SDS–PAGE) in 1× running buffer. The gel was stained with Imperial Protein Stain (Pierce).

Single-molecule TIRFM

Single-molecule measurements were carried out using Prism type TIRFM as previously described (32). Cy3 fluorescence was excited by a DPSS laser (532 nm, 75mW, Coherent), whereas diode laser (641 nm, 100 mW, Coherent) was used for direct excitation of Cy5. The fluorescence signals originated from the Cy3 and Cy5 dyes were collected by a water immersion objective 60× (Olympus), separated by a 630-nm dichroic mirror, passed through a 550-nm long-pass filter to block out laser scattering and detected by EMCCD camera (Andor) with a time resolution of 30 ms.

Reaction conditions for the single-molecule assay

FBH1–bio was immobilized on a quartz surface (Finkenbeiner) coated with polyethylene glycol to eliminate non-specific surface adsorption (Figure 1A). The immobilization was mediated by biotin–neutravidin interaction between biotinylated protein, neutravidin (Pierce) and biotinylated polymer (PEG-MW: 5000; Nectar Therapeutics). All measurements were performed in 50 mM Tris–HCl (pH 7.5), 150 mM NaCl, 10% glycerol, 1 mg/ml of trolox (6-hydroxy-2,5,7,8-tetramethylchroman-2-carboxylic acid; Sigma-Aldrich), 1 mg/ml of glucose oxidase (Sigma-Aldrich), 0.4% (w/v) D-glucose (Sigma-Aldrich), 1% v/v 2-mercaptoethanol (Sigma-Aldrich) and 0.04 mg/ml of catalase (Calbiochem). Immobilization of 1:50 dilution of FBH1–bio protein with single-molecule buffer allowed for detection of 100–600 individual molecules per experiment. One nanomolar of Cy3- and Cy5-labeled DNA substrates was flowed into the reaction chamber with or without 1 mM $MgCl_2$ and 1 mM ATP. To identify surface-tethered Ub FBH1 proteins, TMR-TUBE2 (Lifesensor) was used at 1:5000 dilution. TMR-TUBE2 has a single-TAMRA fluorophore ($\lambda_{EX,\ max}$ = 540 nm, $\lambda_{EM,\ max}$ = 578 nm) attached to the tandem ubiquitin-binding entities with his_6 tag. It is excited and detected in the same spectral window as Cy3.

RAD51 nucleoprotein filaments

To assemble RAD51 nucleoprotein filaments, 1 nM [60 nM (nucleotides)] Cy3/Cy5 dually labeled poly$(dT)_{60}$ (Supplementary Tables S1 and S2) was combined with 40 nM human RAD51 protein and pre-incubated for 30 min at room temperature in the buffer containing 50 mM Tris–HCl (pH 7.5), 150 mM NaCl, 10% glycerol, 1 mM ATP, 5 mM $MgCl_2$ and 5 mM $CaCl_2$. To completely saturate ssDNA with RAD51, the molar ratio for ssDNA (nucleotides):RAD51 (molecules) was set as 3:2. After pre-incubation, RAD51 filaments were diluted in the imaging buffer, and their interaction with surface-tethered FBH1 was analyzed similar to that of the protein-free DNA substrates.

Sorting ubiquitylated and non-ubiquitylated FBH1 molecules

The single-molecule sorting was carried out in a flow experiment in the open-ended fluid chamber (21). This chamber allows us changing the sample solutions during measurement without any impact on the slide. First, solution containing fluorescently labeled DNA or RAD51–ssDNA nucleoprotein filament was infused in the chamber, and the functional assays were carried out. Then, the DNA solution was exchanged with the buffer containing 1:5000 dilution of TMR-TUBE2 (LifeSensors). After 2–5 min incubation, the TMR-TUBE2 solution was replaced with the buffer to remove unbound TUBE2s. Trajectories originated from Ub FBH1 molecules were distinguished from non-ubiquitylated (non-Ub) FBH1 because of the presence of bound TMR-TUBE2. The 1:5000 dilution of TMR-TUBE2 reagent was selected after testing a range of dilutions and corresponds to the inflection point of the correlation between the fraction of TMR-TUBE2 positive trajectories and the reagent concentration. Lower concentrations of TMR-TUBE2 lead to underestimation of the Ub FBH1 population. Higher concentrations, on the other hand, may cause some background fluorescence. The selectivity of TMR-TUBE2 for Ub FBH1 was confirmed by staining of the PEG-pacified TIRFM surface in the absence of FBH1 and by using unmodified FBH1.

Data acquisition and analysis

Single-molecule trajectories were extracted from the recorded video file using in-house IDL software. Förster resonance energy transfer (FRET) efficiencies were calculated as the ratio between the acceptor intensity and the total intensity (sum of donor intensity and acceptor intensity). After visually inspecting the acquired data, each event was measured in MATLAB. For the protein-free DNA substrates, the extracted dwell times were binned with the bin size 0.25 s, plotted as histograms and fitted using GraphPad Prism 4.0 software to single-exponential to extract respective rate constants. Because of the smaller number of events collected for the RAD51 nucleoprotein filaments and longer dwell times, the bin size was increased to 2.5. Using MATLAB program, we measured 'on' and 'off' dwell times to yield distributions. The dissociation rates were then calculated by fitting the dwell time distributions to single-exponential decay, yielding the apparent dissociation rate constants k_{off} (s^{-1}). The apparent association rate constants, k_{on} ($M^{-1}s^{-1}$), were calculated as the number of events per second divided by the substrate concentration. $K_d = k_{off}/k_{on}$ (M). The unwinding times were plotted as histograms and fitted to modified Γ function as described in the 'Results' section.

RESULTS

Experimental system for analysis and sorting of individual FBH1 helicase molecules

Immobilization of FBH1 on the flow cell surface provides a means of observing multiple cycles of substrate binding and processing by each helicase molecule within the field of view. Typically, 200–600 molecules can be simultaneously observed. To facilitate surface tethering, FBH1 helicase was produced and biotinylated in HEK293T cells. HEK293 cells were selected because these cells allow for high-efficiency transfection with multiple plasmids and carry out all biochemical machinery involved in post-translational processing of expressed proteins. The minimum and the most efficient recognition sequence for the *E. coli* BirA biotin ligase [BAP; GLNDIFEAQKIEWHW; the underlined lysine residue is biotinylated (33)] was incorporated at the C-terminus of FBH1 protein expressed using previously published construct for expression of FLAG-tagged FBH1 (18) (Supplementary Figure S1A). HEK293T cells were transiently transfected with the plasmid for expression of FLAG-tagged and FBH1–bio using a polyethylenimine-based method (26,27,34). FBH1 was purified using anti-FLAG antibody-conjugated agarose beads. The purified protein contained a covalently attached biotin moiety (Supplementary Figure S1B) and maintained its DNA-dependent ATPase and duplex DNA unwinding activity (Supplementary Figure S1C and D).

Surface-tethered FBH1 displays a *bona fide* DNA helicase activity

We surface-tethered the FBH1–bio and investigated its ability to bind and unwind DNA substrates that were fluorescently labeled with Cy3 and Cy5 dyes (Figure 1A). First, FBH1 activity was tested using simple PD containing 22-bp double-stranded region with 3′ $(dT)_{10}$ overhang (Supplementary Tables S1 and S2). In this substrate, the Cy3 dye was incorporated at the 3′ terminus of the translocation strand, and Cy5 was on the 5′ terminus of the displaced strand near the dsDNA–ssDNA junction. The flow cell was illuminated with 532-nm laser in a TIRFM mode, resulting in direct excitation of Cy3 dyes present within the evanescent field. In this experimental arrangement, the substrate molecules outside of the excitation field are not excited; therefore, they do not contribute to the fluorescence signal. Hence, the fluorescence signal is observed only when a labeled DNA molecule binds to the surface-tethered FBH1–bio. The signal observed in the Cy3 emission channel is due to the direct excitation of Cy3, whereas the signal in the Cy5 emission channel arises from the FRET between Cy3 and Cy5 dyes. The spatial proximity of the two dyes in the intact substrate results in high-FRET efficiency (~0.7). During the course of the experiment, the same FBH1 molecule binds, unwinds and releases multiple DNA molecules, yielding a fluorescence trajectory such as one depicted in the Figure 1B. Consistently observing such trajectories confirmed that tethering FBH1–bio helicase on the surface of the TIRFM flow cell allows following individual FBH1 helicase molecules undergoing repeating cycles of DNA binding and rearrangement over an extended period. Our experimental scheme also allowed us to account not only for productive unwinding events but also for events that did not result in significant substrate rearrangement and are typically overlooked in the traditional bulk experiments. For example, in the absence of ATP, FBH1 readily binds PD with the K_d of 58.2 ± 9.3 nM (Table 1). Fueled by ATP hydrolysis, FBH1 separates the duplex, which increases the distance between Cy3 and Cy5 dyes (Figure 1C–E). In the presence of Mg^{2+} and ATP, the two types of events were observed: (i) binding followed by dissociation (with the K_ds of 40.6 ± 2.5 nM) and (ii) binding followed by unwinding and release of the products (Figure 1C). Although both types of events were observed, nearly a quarter of all detected events resulted in the duplex unwinding confirming that the surface-tethered FBH1 displays a robust *bona fide* helicase activity (Table 2).

Table 1. Substrate binding by FBH1

substrate	k_{on} (10^7 $M^{-1}s^{-1}$)	k_{off} (s^{-1})	K_d (nM)
PD	1.41 ± 0.22	0.82 ± 0.03	58.2 ± 9.3
RFL	1.17 ± 0.11	0.62 ± 0.03	53.0 ± 5.6
PD + ATP	2.17 ± 0.09	0.88 ± 0.04	40.6 ± 2.5
RFL + ATP	3.71 ± 0.18	0.59 ± 0.04	15.9 ± 7.8
RAD51–ssDNA	2.7 ± 0.12	0.18 ± 0.01	6.7 ± 0.5

The errors for the k_{off} constants are the standard errors from fitting the dwell time distribution.
The errors for the k_{on} constants are the standard errors from average.
Errors for K_d's were calculated as $\Delta(K_d) = K_d * \sqrt{\left(\frac{\Delta K_{off}}{K_{off}}\right)^2 + \left(\frac{K_{on}}{\Delta K_{on}}\right)^2}$

FBH1 displays repetitive shuttling on the branched DNA substrates resembling stalled replication forks

In addition to the simple PD substrate resembling a broken arm of a collapsed replication fork, we constructed a DNA substrate that resembles a stalled replication fork (RFL) (Figure 2). The Cy3 and Cy5 fluorophores were positioned so that we could monitor unwinding of the oligo representing the Okazaki fragment. In the absence of ATP, FBH1 bound RFL and PD with similar affinities; however, affinity for the RFL was slightly increased in the presence of ATP (Table 1).

Interestingly, distribution of dwell times (Δt_{total}) showed clear difference between PD1 and RFL (Figure 2C and D). In the case of PD1, we observed simple unwinding events with short exponentially distributed dwells before and after unwinding, and short binding events. In contrast, 23.9% of events for RFL were longer than >5 s, whereas only 3.0% of events for PD1 were longer than >5 s. Many of the longer activity bursts on the RFL substrates showed repetitive change in the FRET efficiency (Figure 2G). We interpreted these events as binding of FBH1 at the fork with its motor core positioned to translocate in the 3′–5′ direction on the 'lagging strand' between the junction and Okazaki fragment. In repetitive cycles, the motor core of the

Table 2. Activities of ubiquitylated and non-ubiquitylated FBH1

substrate	PD		RFL		
	Ub	Non-Ub	Ub	Non-Ub	
Fraction of molecules	27.3	72.7	29.8	70.2	%
k_{on}	1.48 ± 0.15[a]	2.17 ± 0.09[a]	3.75 ± 0.35[a]	3.71 ± 0.18[a]	10^7 $s^{-1}M^{-1}$
k_{step}	5.59 ± 0.79[a]	5.12 ± 0.48[a]	ND	ND	s^{-1}
Bind	77.1	71.7	54.8	51.6	%
Unwind	18.2	22.9	20.5	24.9	
Shuttle and unwind	0	1.1	4.8	3.3	
Shuttle	4.7	4.4	20.0	20.2	
Total	100	100	100	100	

[a]Values for k_{on} and k_{step} are shown as best fitted value ± standard error.

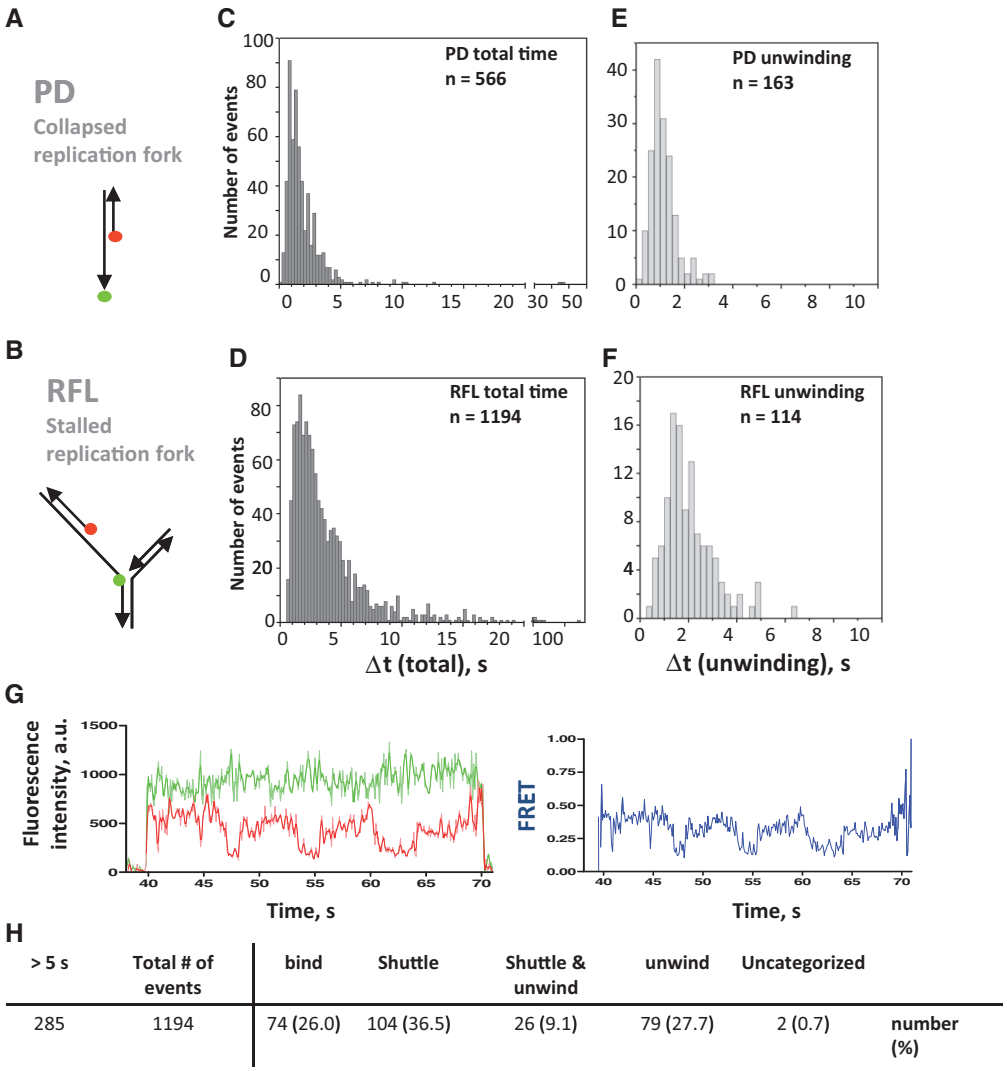

Figure 2. DNA structure influences FBH1 unwinding and translocation behaviors. (**A** and **B**) Schematic representation of the PD1 and RFL substrates, respectively. (**C–F**) Distributions of Δt_{total} (C and D) and $\Delta t_{unwinding}$ (E and F) for PD (upper panels) and RFL (lower panels). All dwell times were binned with the 0.25-s bin size. (**G**) A particular repetitive shuttling trajectory and FRET value for RFL. (**H**) Classification and percentage of each event over longer event (Δt_{total} >5 s) for RFL.

helicase then shuttles on the single-stranded region while the helicase remains bound to the junction. The shuttling may be accounted for by translocation of the helicase on the single strand, but it may also include partial unwinding of the Okazaki fragment. The occurrence of binding, unwinding and shuttling events, which are longer than >5 s, for RFL substrates is summarized in Figure 2H. Repetitive movement was previously observed for other

SF1 helicases (22,23), and in the case of FBH1, it may play an anti-recombinogenic role by preventing RAD51 recombinase from assembling into the nucleoprotein filament.

The N-terminal domain of FBH1 contains an auxiliary DNA-binding site

We postulated that the feature responsible for both duplex unwinding and for anchoring of the helicase to the fork likely resides within the large N-terminal region of FBH1 (Supplementary Figure S1A). To test this hypothesis, we purified the F-box–containing N-terminal domain ($FBH1^{NTD}$: 1–351 residue) (Figure 3A) and probed its DNA-binding activity (Figure 3B). Purified $FBH1^{NTD}$ displayed a weak DNA binding to both ssDNA and dsDNA, suggesting that it indeed contains a DNA binding site.

RAD51 physically interacts with the N-terminal domain of FBH1

FBH1 may use its DNA translocase activity to prevent recombination events by interfering with assembly of or dismantling RAD51–DNA complexes (7–10). Although less likely, FBH1 may also target RAD51 for the SCF^{FBH1}-mediated ubiquitylation. Either of these two activities would depend on the physical interaction between FBH1 and RAD51. We expected the RAD51-binding locus to reside within the N-terminal region of FBH1. Using the Ni-NTA pull-down assays, we showed that $FBH1^{NTD}$ does indeed interact with RAD51 protein (Figure 3C), which may reflect the interaction between FBH1 and RAD51 nucleoprotein filament functionally important for the anti-recombinogenic function of FBH1.

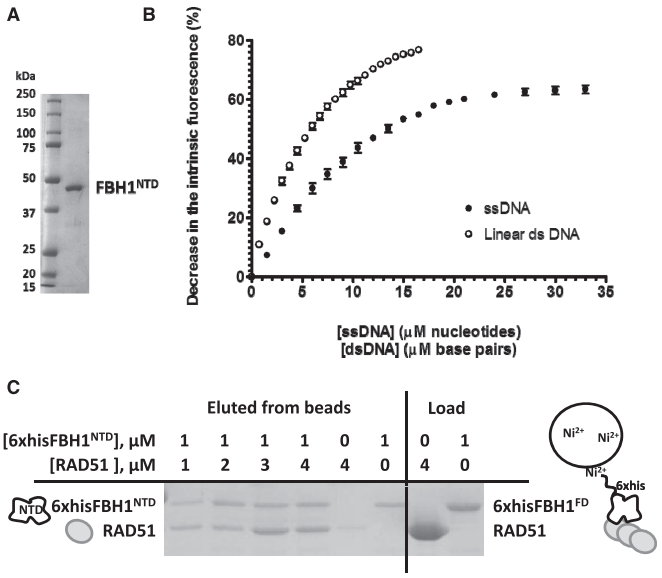

Figure 3. $FBH1^{NTD}$ interacts with ssDNA, dsDNA and RAD51. (**A**) SDS–PAGE of purified $FBH1^{NTD}$ visualized by Coomassie brilliant blue staining. N-terminal his-tagged and C-terminal FLAG-tagged $FBH1^{NTD}$ is expressed as 371 amino acids (42 kDa) polypeptide. Purification procedure outlined in the Supplementary Methods yielded a pure $FBH1^{NTD}$ protein of expected molecular weight. (**B**) To determine whether $FBH1^{NTD}$ contains secondary DNA-binding site, we tested its ability to interact with ssDNA and dsDNA by following changes in the intrinsic fluorescence of the aromatic residues. We observed the most profound difference between $FBH1^{NTD}$ fluorescence in the absence and in the presence of DNA by exciting it at 280 nm and following fluorescence at 320 nm. This fluorescence change indicates change in the hydrophobic environment of aromatic residues, and thereby it can be used as an indicator of the DNA binding. (**C**) Interaction between the 6× his-tagged $FBH1^{NTD}$ and RAD51 protein was investigated using pull-down on Ni-NTA beads. SDS–PAGE shows the proteins co-eluted from the beads.

FBH1 forms stable complexes with RAD51 nucleoprotein filament

To probe the FBH1–RAD51 interaction at the single-molecule level, we investigated binding of RAD51 nucleoprotein filament assembled on the ssDNA dually labeled with Cy3 and Cy5 dyes by the surface-tethered FBH1 (Figure 4A). Similar to the protein-free DNA substrates described earlier in the text, binding of the individual RAD51 filaments was inferred from the appearance of the fluorescent signal in both Cy3 and Cy5 channels (Figure 4B). The dually labeled substrate was used to ensure that fully formed RAD51 filaments were successfully assembled (Figure 4A): in the presence of Ca^{2+} and ATP, RAD51 forms 'active' and stable nucleoprotein filament, which extends ssDNA 1.6-fold beyond B-form (35,36). This is reflected in a low FRET between the two dyes (Figure 4A and C). The extended form of the RAD51 filament (stable FRET ~0.2) was observed in most (90%) of the FBH1-bound species, suggesting that binding without remodeling of the nucleoprotein filament occurs under the selected conditions. The distribution of the ON dwell times was fitted to a single exponential, yielding the apparent dissociation rate constant $k_{off} = 0.18 \pm 0.01\,s^{-1}$. The apparent association rate constant was calculated from the number of binding events per unit of time to be $k_{on} = (2.7 \pm 0.12)*10^7\,s^{-1} \times M^{-1}$. The ratio of the two rate constants yielded an equilibrium dissociation constant $K_d = 6.7 \pm 0.5$ nM, which is significantly tighter than that for the protein-free PD and RFL substrates (Table 1).

Simultaneous analysis and sorting of unmodified and post-translationally modified FBH1 molecules

FBH1 plays a role in assembling of ubiquitin polymer as a component of SCF^{FBH1} (Skp1–Cul1–F-box protein) E3 ubiquitin ligase (18,20) and is a target of the DNA damage-induced ubiquitylation (9). We applied our new single-molecule sorting technique to quantify, simultaneously probe and distinguish activities of Ub and non-Ub FBH1 molecules. To increase the fraction of ubiquitylated FBH1, the plasmid for expression of HA-tagged ubiquitin (25) was added to the co-transfections (Supplementary Figure S1B). During the expression process in HEK293T cells, endogenous cellular ubiquitin ligases (likely the SCF^{FBH1}) modify a fraction of FBH1 molecules, yielding a mixed pool of Ub and non-Ub enzymes (Supplementary Figure S1B). After completing the functional analysis, molecules containing poly-ubiquitin chains were identified because of their ability to bind TMR-TUBE2. TMR-TUBE2 is a TAMRA-labeled tandem ubiquitin-binding moiety, a reagent developed to bind poly-ubiquitin chains with

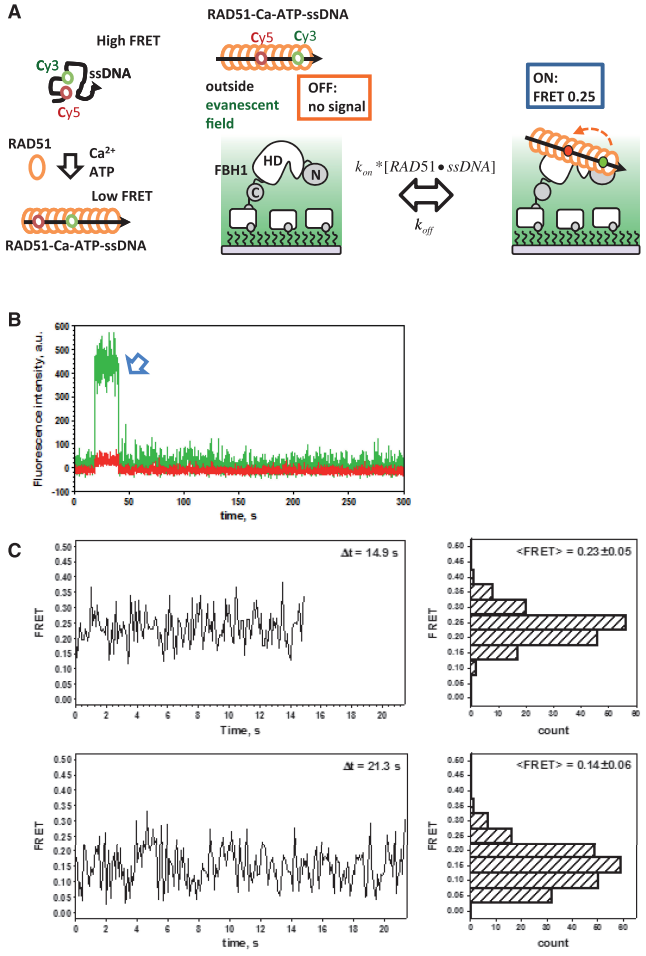

Figure 4. Immobilized FBH1 interacts with RAD51 nucleoprotein filament. (**A**) Schematic representation of TIRFM-based assay for analysis of the RAD51 nucleoprotein filament binding by the individual surface-tethered helicases molecules. The experimental strategy is similar to that described for the DNA substrates, except the preformed nucleoprotein filaments assembled by RAD51 recombinase on the 60mer ssDNA were used as a substrate. Appearance of the fluorescence in both Cy3 and Cy5 channels corresponds to the nucleoprotein filament binding by the immobilized FBH1; the low FRET between the two dyes confirms that the nucleoprotein filament is fully formed and is in the extended (active) conformation. (**B**) Activity of an individual surface-tethered FBH1 molecule was monitored for >200 s. Blue arrow indicates RAD51 filament-binding event. (**C**) Representative FRET trajectories of two binding events. FRET values were calculated from the Cy3 and Cy5 intensities exactly as described for the DNA substrates (left) and binned in 0.05 U intervals for each event (right) using GraphPad Prism 4.0.

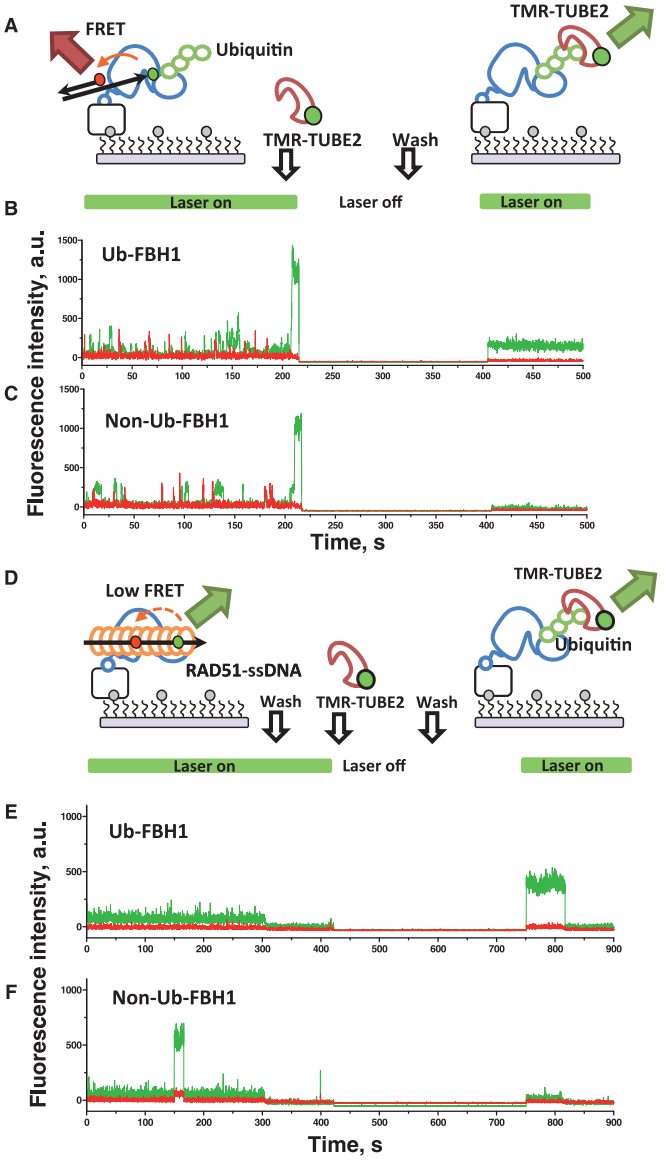

Figure 5. Sorting of ubiquitylated and non-ubiquitylated FBH1 molecules. (**A**) Schematic representation of the single-molecule sorting experiment. (**B**) Representative trajectory for ubiquitylated FBH1 in the presence of 1 mM ATP, 3 mM $MgCl_2$ and 1 nM PD1. Time points at which the DNA substrate was exchanged with TMR-TUBE2, when unbound TMR-TUBE2 was washed out of the flow cell and when the laser was switched off and on are indicated over the trajectory. (**C**) Representative trajectory of unmodified FBH1 from the same experiment. (**D**) Schematic representation of the single-molecule sorting experiment with RAD51 nucleoprotein filament used as a substrate. (**E**) Representative trajectory of the ubiquitylated FBH1 in the presence of 1 mM ATP, 5 mM $MgCl_2$, 5 mM $CaCl_2$, 40 nM RAD51 and 1 nM Cy3/Cy5-labeled poly(dT)$_{60}$. Time points at which the DNA substrate was exchanged with TMR-TUBE2, when unbound TMR-TUBE2 was washed out of the flow cell and when the laser was switched off and on are indicated over the trajectory. (**F**) Representative trajectory of unmodified FBH1 from the same experiment.

high affinity and specificity. TMR-TUBE2 replaced the DNA substrate in the flow cell. After a brief incubation to allow binding to the poly-ubiquitin chains on the immobilized FBH1, the excess of TMR-TUBE2 was removed from the flow cell. The TMR fluorescence was then excited with the green laser. Only FBH1 molecules containing poly-ubiquitin chains were visible at this point (compare Figure 5B and C). The TMR-TUBE2 concentration used in this experimental scheme was optimized to saturate and reveal all ubiquitylated helicase molecules. Although poly-ubiquitylation is readily revealed by staining with TMR-TUBE2, fluorescently labeled antibodies can be used to visualize and quantify other types of modifications.

TMR-TUBE2 staining allowed us to correlate the fundamental activities of the helicase to its modification state. Each trajectory, which displayed a signal in the Cy3

Table 3. Affinities of ubiquitylated and non-ubiquitylated FBH1 for Rad51 nucleoprotein filament

substrate	T_{60}•RAD51$^{Ca/Mg/ATP}$		
	Ub	Non-Ub	
Fraction of molecules	36.5	63.5	%
k_{on}	0.69 ± 0.18[a]	2.7 ± 0.12[a]	10^7 $s^{-1}M^{-1}$
k_{off}	0.11 ± 0.12[a]	0.18 ± 0.01[a]	s^{-1}
K_d (nM)	16 ± 4.5	6.7 ± 0.5	nM

[a]The errors for the k_{off} constants are the standard errors from fitting the dwell time distribution.
The errors for the k_{on} constants are the standard errors from average.
Errors for K_ds were calculated as $\Delta(K_d) = K_d * \sqrt{\left(\frac{\Delta K_{off}}{K_{off}}\right)^2 + \left(\frac{K_{on}}{\Delta K_{on}}\right)^2}$

channel after the DNA substrates were replaced with TMR-TUBE2, was classified as Ub FBH1 molecule (Figure 5). The percentage of Ub FBH1 and non-Ub FBH1 was approximately 30 and 70%, respectively (Tables 2 and 3). The ubiquitylated molecules were able to bind, translocate and unwind the Cy3/Cy5-labeled DNA substrates in a manner essentially identical to that of the non-Ub FBH1 (Figure 5B and C and Table 2). Notably, ubiquitylation had only a minor effect on the FBH1 activities on the protein-free DNA substrates (Table 2); it slightly decreased the fraction of unwinding events on both PD1 and RFL substrates. In contrast, ubiquitylation affected interaction between FBH1 and RAD51. FBH1 showed a dramatically reduced affinity for the RAD51 nucleoprotein filament compared with the unmodified helicase because of the reduction in k_{on} from 2.7 ± 0.12 to 0.69 ± 0.18 s^{-1} (Figure 5D and F and Table 3). The few recorded events of RAD51 filament binding to the ubiquitylated FBH1 yielded similar k_{off} for the Ub-FBH1•RAD51 filament, suggesting that ubiquitylation interferes with FBH1 binding to the RAD51 nucleoprotein filament, but not with the stability of the complex when it is formed.

DISCUSSION

Maintaining integrity of the genome and its faithful duplication involves a protein network in which a stochastic combination of PTMs and molecular association yields complexes adapted to repair numerous types of DNA damage or to resolve cytotoxic DNA repair intermediates. PTMs tune activities and interactions of their targets and broaden the range of repairable DNA lesions. It is likely that a small fraction of a DNA repair protein carrying out an activating or modifying PTM may greatly influence cellular fate. Biochemical characterization of such an influence is commonly hampered by difficulty in isolating a small fraction of modified protein from the population of unmodified protein. As a result, an important modification as well as its effect on the protein functions and interactions may be easily overlooked when the biochemical properties are averaged over the whole-cellular pool. Here, we developed a method, which allows us to quantify the fraction of the DNA repair protein modified in the cell and to separate activities of the post-translationally modified proteins from unmodified counterparts.

The first step in our single-molecule sorting methodology is production of the protein of interest (exemplified in this study by FBH1 helicase) in human cells and its immobilization on the surface of the TIRFM flow cell. Even though the immobilized helicase is invisible to us, its location on the surface of the flow cell can be triangulated based on the activity trajectory originating from that particular location. The experimental arrangement where the helicase is immobilized and the fluorescent substrate is free in solution, allows us to overcome one of the main concerns associated with single-molecule TIRFM studies, namely, the photo-bleaching of the dyes incorporated into the substrate. When the helicase is immobilized, each DNA-binding and rearrangement event involves a new DNA substrate that has not been excited before, thus allowing one to collect long fluorescence trajectories containing multiple activity events. The substrate is then replaced with the fluorescently labeled moiety, which specifically binds and forms a stable complex with the PTM or with the modified form of the protein.

In contrast to *Schizosaccharomyces pombe* Fbh1, whose anti-recombinogenic role is well-established (7–9), human FBH1 was proposed to function as both pro- and anti-recombinase (6). The ability to antagonize recombination is generally inferred by analogy with the *S. pombe* and *Ustilago maydis* homologues and overlaps, at least in part, with the functions of BLM helicase (12,37), which protects stalled replication forks as well as FANCJ (38), RTEL1 (39) and PARI (40) enzymes that were proposed to antagonize homologous recombination by inhibiting or dismantling RAD51 nucleoprotein filament. The pro-recombinogenic activity is specific to vertebrate FBH1 and is associated with production of long stretches of ssDNA in response to replication stress (6). It is expected, therefore, to be driven by the *bona fide* helicase activity of FBH1. As PTMs may directly influence activity of DNA repair enzymes, we expected that ubiquitylation of FBH1 may modify its activities and/or its interactions. We, therefore, used FBH1 to establish the sorting methodology. The presence of poly-ubiquitin chains on FBH1 molecules was revealed by staining with TMR-TUBE2 *in singulo* (Figure 5). We demonstrated that ubiquitylation had minimal effects on either the helicase activity of FBH1 or its ability to translocate on ssDNA. This result agreed with the finding by Fugger *et al.* (6) that both unmodified and poly-ubiquitylated forms of FBH1 should be able to generate ssDNA, which can serve as a substrate for RAD51 filament formation and to activate ATM-mediated signaling; both forms should also be able to use the translocase activity to protect the replication fork (Table 2). In contrast to the strand separation and translocase activities, poly-ubiquitylation of FBH1 interfered with RAD51 nucleoprotein filament binding by the modified helicase (Figure 5 and Table 3).

Fugger *et al.* demonstrated that overexpression of the F-box mutant (L278A and P79A) reduced RAD51, but not RPA foci formation in the hydroxyurea-treated cells.

At the same time, helicase-deficient mutant (D698N) attenuated RAD51 foci formation because of significant reduction in ssDNA formation (6). The F-box mutant likely prevents poly-ubiquitylation of FBH1 by SCF^{FBH1}, yielding the unmodified FBH1 capable of interacting with and dismantling RAD51 nucleoprotein filaments, as only unmodified FBH1 helicase interacts with RAD51, which is consistent with the reduction in the RAD51 foci formation. In contrast, ubiquitylation does not affect the helicase activity of FBH1 and ensuing appearance of the RPA foci. By restricting the FBH1–RAD51 interaction, ubiquitylation may promote RAD51-mediated activities observed by Petermann *et al.* (24) on both the collapsed and on the repairable replication forks stalled by hydroxyurea treatment. Our results suggested that ubiquitylation is used both to restrict the anti-recombinogenic activity of FBH1 and its abundance in living cells.

The methodology we developed will improve our ability to quantify post-translational modifications and evaluate their effect on the activities of the DNA repair and maintenance proteins. It will also lay the ground for future reconstitutions of the DNA repair and recombination networks in their full complexity.

SUPPLEMENTARY DATA

Supplementary Data are available at NAR Online: Supplementary Tables 1 and 2 and Supplementary Figure 1.

ACKNOWLEDGEMENTS

The authors thank Dr Marc Wold, Dr M. Todd Washington, Dr M. Ashley Spies, Dr Colin Wu, Dr Masayoshi Honda, Shyamal Subramanyam and William Jones for critically reading the manuscript and Mr Gordon Lee for the help with $FBH1^{NTD}$ purification.

FUNDING

HHMI Early Career Scientist Award and American Cancer Society [RSG-09-182-01-DMC to M.S.]. Funding for open access charge: University of Iowa Carver College of Medicine start-up funds.

Conflict of interest statement. None declared.

REFERENCES

1. Walsh,C.T., Garneau-Tsodikova,S. and Gatto,G.J. Jr (2005) Protein posttranslational modifications: the chemistry of proteome diversifications. *Angew Chem. Int. Ed. Engl.*, **44**, 7342–7372.
2. Thomson,T.M. and Guerra-Rebollo,M. (2010) Ubiquitin and SUMO signalling in DNA repair. *Biochem. Soc. Trans.*, **38**, 116–131.
3. van Kasteren,S. (2012) Synthesis of post-translationally modified proteins. *Biochem. Soc. Trans.*, **40**, 929–944.
4. Matos,J., Blanco,M.G., Maslen,S., Skehel,J.M. and West,S.C. (2011) Regulatory control of the resolution of DNA recombination intermediates during meiosis and mitosis. *Cell*, **147**, 158–172.
5. Honda,M., Okuno,Y., Yoo,J., Ha,T. and Spies,M. (2011) Tyrosine phosphorylation enhances RAD52-mediated annealing by modulating its DNA binding. *EMBO J.*, **30**, 3368–3382.
6. Fugger,K., Mistrik,M., Danielsen,J.R., Dinant,C., Falck,J., Bartek,J., Lukas,J. and Mailand,N. (2009) Human Fbh1 helicase contributes to genome maintenance via pro- and anti-recombinase activities. *J. Cell Biol.*, **186**, 655–663.
7. Osman,F., Dixon,J., Barr,A.R. and Whitby,M.C. (2005) The F-Box DNA helicase Fbh1 prevents Rhp51-dependent recombination without mediator proteins. *Mol. Cell. Biol.*, **25**, 8084–8096.
8. Morishita,T., Furukawa,F., Sakaguchi,C., Toda,T., Carr,A.M., Iwasaki,H. and Shinagawa,H. (2005) Role of the Schizosaccharomyces pombe F-Box DNA helicase in processing recombination intermediates. *Mol. Cell. Biol.*, **25**, 8074–8083.
9. Chiolo,I., Saponaro,M., Baryshnikova,A., Kim,J.H., Seo,Y.S. and Liberi,G. (2007) The human F-Box DNA helicase FBH1 faces Saccharomyces cerevisiae Srs2 and postreplication repair pathway roles. *Mol. Cell. Biol.*, **27**, 7439–7450.
10. Lorenz,A., Osman,F., Folkyte,V., Sofueva,S. and Whitby,M.C. (2009) Fbh1 limits Rad51-dependent recombination at blocked replication forks. *Mol. Cell. Biol.*, **29**, 4742–4756.
11. Antony,E., Tomko,E.J., Xiao,Q., Krejci,L., Lohman,T.M. and Ellenberger,T. (2009) Srs2 disassembles Rad51 filaments by a protein-protein interaction triggering ATP turnover and dissociation of Rad51 from DNA. *Mol. Cell*, **35**, 105–115.
12. Kohzaki,M., Hatanaka,A., Sonoda,E., Yamazoe,M., Kikuchi,K., Vu Trung,N., Szuts,D., Sale,J.E., Shinagawa,H., Watanabe,M. *et al.* (2007) Cooperative roles of vertebrate Fbh1 and Blm DNA helicases in avoidance of crossovers during recombination initiated by replication fork collapse. *Mol. Cell. Biol.*, **27**, 2812–2820.
13. Laulier,C., Cheng,A., Huang,N. and Stark,J.M. (2010) Mammalian Fbh1 is important to restore normal mitotic progression following decatenation stress. *DNA Repair*, **9**, 708–717.
14. Lohman,T.M., Tomko,E.J. and Wu,C.G. (2008) Non-hexameric DNA helicases and translocases: mechanisms and regulation. *Nat. Rev. Mol. Cell Biol.*, **9**, 391–401.
15. Tuteja,N. and Tuteja,R. (2004) Unraveling DNA helicases. Motif, structure, mechanism and function. *Eur. J. Biochem.*, **271**, 1849–1863.
16. Gorbalenya,A.E. and Koonin,E.V. (1993) Helicases: amino acid sequence comparisons and structure-function relationships. *Curr. Opin. Struct. Biol.*, **3**, 419–429.
17. Singleton,M.R., Dillingham,M.S. and Wigley,D.B. (2007) Structure and mechanism of helicases and nucleic acid translocases. *Annu. Rev. Biochem.*, **76**, 23–50.
18. Kim,J., Kim,J.H., Lee,S.H., Kim,D.H., Kang,H.Y., Bae,S.H., Pan,Z.Q. and Seo,Y.S. (2002) The novel human DNA helicase hFBH1 is an F-box protein. *J. Biol. Chem.*, **277**, 24530–24537.
19. Park,J.S., Choi,E., Lee,S.H., Lee,C. and Seo,Y.S. (1997) A DNA helicase from Schizosaccharomyces pombe stimulated by single-stranded DNA-binding protein at low ATP concentration. *J. Biol. Chem.*, **272**, 18910–18919.
20. Kim,J.H., Kim,J., Kim,D.H., Ryu,G.H., Bae,S.H. and Seo,Y.S. (2004) SCFhFBH1 can act as helicase and E3 ubiquitin ligase. *Nucleic Acids Res.*, **32**, 2287–2297.
21. Roy,R., Hohng,S. and Ha,T. (2008) A practical guide to single-molecule FRET. *Nat. Methods*, **5**, 507–516.
22. Myong,S., Rasnik,I., Joo,C., Lohman,T.M. and Ha,T. (2005) Repetitive shuttling of a motor protein on DNA. *Nature*, **437**, 1321–1325.
23. Park,J., Myong,S., Niedziela-Majka,A., Lee,K.S., Yu,J., Lohman,T.M. and Ha,T. (2010) PcrA helicase dismantles RecA filaments by reeling in DNA in uniform steps. *Cell*, **142**, 544–555.
24. Petermann,E., Orta,M.L., Issaeva,N., Schultz,N. and Helleday,T. (2010) Hydroxyurea-stalled replication forks become progressively inactivated and require two different RAD51-mediated pathways for restart and repair. *Mol. Cell*, **37**, 492–502.
25. Lamb,A., Yang,X.D., Tsang,Y.H., Li,J.D., Higashi,H., Hatakeyama,M., Peek,R.M., Blanke,S.R. and Chen,L.F. (2009) Helicobacter pylori CagA activates NF-kappaB by targeting

TAK1 for TRAF6-mediated Lys 63 ubiquitination. *EMBO Rep.*, **10**, 1242–1249.
26. Durocher,Y., Perret,S. and Kamen,A. (2002) High-level and high-throughput recombinant protein production by transient transfection of suspension-growing human 293-EBNA1 cells. *Nucleic Acids Res.*, **30**, E9.
27. Kichler,A. (2004) Gene transfer with modified polyethylenimines. *J. Gene Med.*, **6**, S3–S10.
28. Kowalczykowski,S.C. and Krupp,R.A. (1987) Effects of *Escherichia coli* SSB protein on the single-stranded DNA-dependent ATPase activity of *Escherichia coli* RecA protein. Evidence that SSB protein facilitates the binding of RecA protein to regions of secondary structure within single-stranded DNA. *J. Mol. Biol.*, **193**, 97–113.
29. Sigurdsson,S., Trujillo,K., Song,B., Stratton,S. and Sung,P. (2001) Basis for avid homologous DNA strand exchange by human Rad51 and RPA. *J. Biol. Chem.*, **276**, 8798–8806.
30. Tombline,G. and Fishel,R. (2002) Biochemical characterization of the human RAD51 protein. *J. Biol. Chem.*, **277**, 14417–14425.
31. Spies,M. and Kowalczykowski,S.C. (2006) The RecA binding locus of RecBCD is a general domain for recruitment of DNA strand exchange proteins. *Mol. Cell*, **21**, 573–580.
32. Honda,M., Park,J., Pugh,R.A., Ha,T. and Spies,M. (2009) Single-molecule analysis reveals differential effect of ssDNA-binding proteins on DNA translocation by XPD helicase. *Mol. Cell*, **35**, 694–703.
33. Beckett,D., Kovaleva,E. and Schatz,P.J. (1999) A minimal peptide substrate in biotin holoenzyme synthetase-catalyzed biotinylation. *Protein Sci.*, **8**, 921–929.
34. Chang,V.T., Crispin,M., Aricescu,A.R., Harvey,D.J., Nettleship,J.E., Fennelly,J.A., Yu,C., Boles,K.S., Evans,E.J., Stuart,D.I. *et al.* (2007) Glycoprotein structural genomics: solving the glycosylation problem. *Structure*, **15**, 267–273.
35. Bugreev,D.V. and Mazin,A.V. (2004) Ca2+ activates human homologous recombination protein Rad51 by modulating its ATPase activity. *Proc. Natl. Acad. Sci. USA*, **101**, 9988–9993.
36. Ristic,D., Modesti,M., van der Heijden,T., van Noort,J., Dekker,C., Kanaar,R. and Wyman,C. (2005) Human Rad51 filaments on double- and single-stranded DNA: correlating regular and irregular forms with recombination function. *Nucleic Acids Res.*, **33**, 3292–3302.
37. Mao,N., Kojic,M. and Holloman,W.K. (2009) Role of Blm and collaborating factors in recombination and survival following replication stress in Ustilago maydis. *DNA Repair*, **8**, 752–759.
38. Sommers,J.A., Rawtani,N., Gupta,R., Bugreev,D.V., Mazin,A.V., Cantor,S.B. and Brosh,R.M. Jr (2009) FANCJ uses its motor ATPase to destabilize protein-DNA complexes, unwind triplexes, and inhibit RAD51 strand exchange. *J. Biol. Chem.*, **284**, 7505–7517.
39. Barber,L.J., Youds,J.L., Ward,J.D., McIlwraith,M.J., O'Neil,N.J., Petalcorin,M.I., Martin,J.S., Collis,S.J., Cantor,S.B., Auclair,M. *et al.* (2008) RTEL1 maintains genomic stability by suppressing homologous recombination. *Cell*, **135**, 261–271.
40. Moldovan,G.L., Dejsuphong,D., Petalcorin,M.I., Hofmann,K., Takeda,S., Boulton,S.J. and D'Andrea,A.D. (2012) Inhibition of homologous recombination by the PCNA-interacting protein PARI. *Mol. Cell*, **45**, 75–86.